Received: 9 May 2021 | Revised: 21 September 2021 | Accepted: 25 September 2021

DOI: 10.1002/mdp2.267

SPECIAL ISSUE ARTICLE

WILEY

The effects of layers orientation on impact energy evaluation of FDM printed specimens

Iulian-Ionut Ailinei | **Sergiu Valentin Galatanu** | **Liviu Marsavina**

Politehnica University of Timişoara, Timişoara, Romania

Correspondence
Sergiu Valentin Galatanu, Politehnica University of Timişoara, 1 Mihai Viteazu Blvd., 300222 Timişoara, Romania.
Email: sergiu.galatanu@upt.ro

Funding information
European Union's Horizon 2020 research and innovation program, Grant/Award Number: 857124

Abstract

This paper investigates the effects of layers orientation on impact energy absorbed by acrylonitrile butadiene styrene (ABS) test specimens, obtained by additive manufacturing (AM), having three in-plane deposition directions (0°, 45°, and 90°). The specimens were tested with instrumented Charpy hammer, CEAST 9050 Pendulum Impact System, according to standard ISO179-1. Unnotched specimens were tested in edgewise direction based on measured velocity and impact force; absorbed energy was computed. The average energy obtained during impact tests for specimens with the orientation of the layers at 45° was about 0.39 J. For those with layer orientation at 0° and 90°, respectively, it was 0.63 and 0.81 J. A hinge break failure mode was observed for 0° and 90° specimens, and brittle fracture for 45° specimens.

KEYWORDS

ABS, Charpy impact, FDM, finite element analysis, impact strength

1 | INTRODUCTION

Nowadays, polymers are a class of materials increasingly used in various applications. The implementation of polymers in the mechanical and functional parts of machines in the automotive and aerospace industries drives the improvement of the mechanical properties of pure polymers. Bilkar et al.[1] have shown that the increase in tensile strength and dimensional accuracy increases with cellulose nanofibers reinforced in acrylonitrile butadiene styrene (ABS). At the same time, fused deposition modeling (FDM) has started to be used more and more in the manufacture of customized components.[2–6] Kumar et al.[7] have shown that three-dimensional (3D) printing with a fill density closer to 100% increases mechanical properties. The higher fill density makes a sample heavier and more solid, providing better strength and high loading capacity. The effects of FDM-3D printing parameters on tensile, flexural, and impact properties of printed PEEK, CF/PEEK, and GF/PEEK samples were investigated in Wang et al.[8] However, the materials made by 3D printing show different mechanical properties in different directions due to the inherent anisotropic features of the printing process.[8–10] The fatigue strength of Ti–6Al–4V circular notched samples produced by SLM was assessed.[11,12] In notched and unnotched conditions, the Charpy impact behavior of three polycarbonate grades is presented in Benedetti et al.[13]

Benedetti et al.[13] show the progress in improving the fatigue performance of metal-based cellular structures manufactured by additive manufacturing (AM) by providing insights and a glimpse into the future for fatigue-tolerant additively manufactured designed cellular materials.

The paper is divided into three sections. The first section presents procedures and results of the Charpy impact tests made on ABS test specimens obtained by AM, having three deposition directions. The second section has shown the numerical simulation results compared to physical tests, while the main conclusions are summarized in the last section.

2 | EXPERIMENTAL INVESTIGATIONS

2.1 | Preparation of test specimens

Three samples were printed in-plane, one sample laying on the XY plane, and have three orientations (Figure 1). For test specimen fabrication, an Ultimaker 3, a 3D printing machine, was used. The most critical parameters that significantly influence sample quality and printing duration are infill percentage and printing resolution. An infill percentage of approximately 100% was chosen to have a uniform mass inside the specimens, and printing resolution was chosen at 0.12 mm with linear increment. An ABS filament with a diameter of 0.25 mm having a temperature of 100°C was used. The printer's plate temperature was 60°C. Infill percentage and printing resolution mentioned above led to a printing time of 10 min per specimen.

The shape and dimensions of specimens, shown in Figure 2, imposed by the Charpy impact testing standard,[14,15] are as follows: length of 55 ± 2 (mm), with 10.0 ± 0.2 (mm) and thickness of 2.5 ± 0.2 (mm).

2.2 | Experimental setup

The Charpy test is the most used method to evaluate material's impact toughness (or relative toughness). It can be used on various types of materials such as polymers, ceramics, and composites. In this study, an Instron CEAST 9050 Charpy test rig was used to determine the impact strength of the 3D printed samples. The equipment consists of a 229.7 (mm) long impact pendulum combined with a 1.186 (kg) hammer at the striker end, holding potential energy of 5 (J) and an impact speed of 2.9 (m/s). The recorded force signal measurements were forwarded to the equipment's computer software via a data acquisition system connected to the hammer. The pendulum is raised to a defined height and released to fall. The difference between the initial and final height of the pendulum is directly proportional to the amount of energy lost due to fracturing the specimen.

Specimens were placed horizontally—in the edgewise manner, on the supports of the test rig and pushed against the anvils by the striker (Figure 2).

2.3 | Experimental results

The experimental tests have been performed for nine unnotched specimens obtained by AM, having three deposition directions, to determine the impact characteristics. The standard to be followed for plastics, the ISO 179,[16] which covers

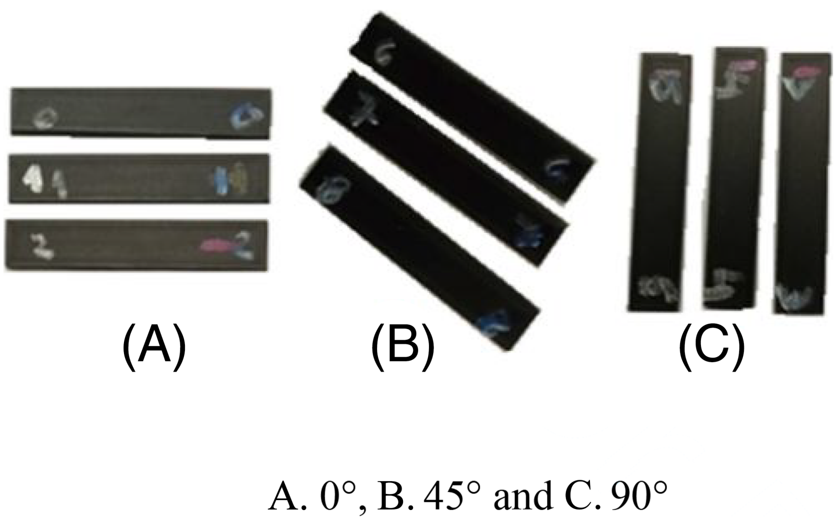

FIGURE 1 3D printing test specimens

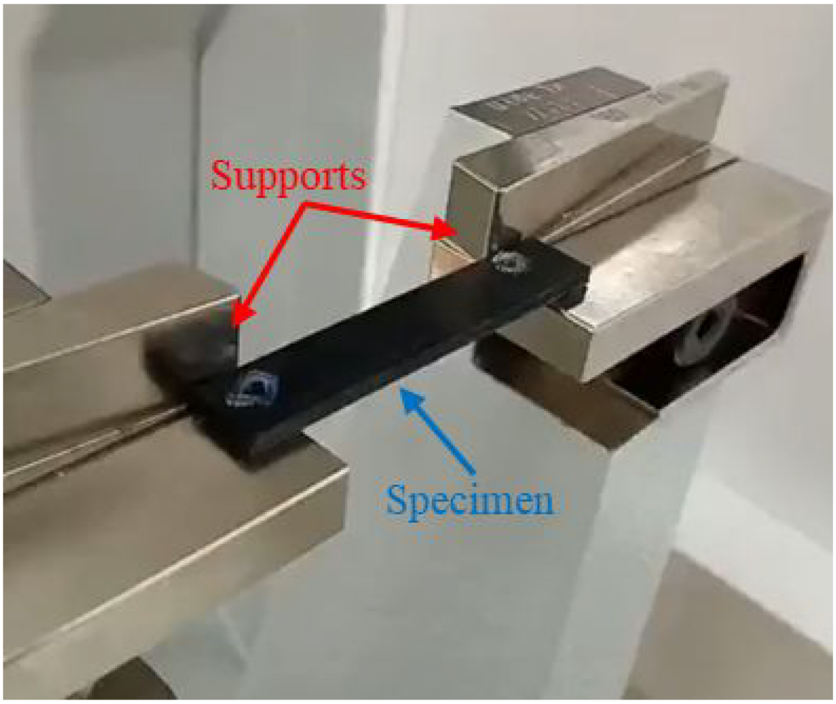

FIGURE 2 Placing specimen on supports to be tested

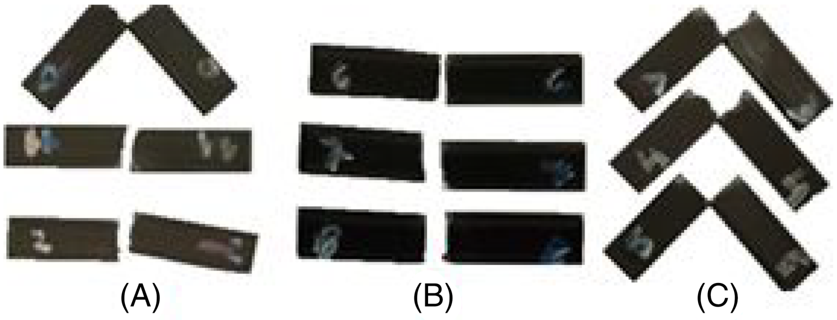

A. 0°, B. 45° and C. 90°

FIGURE 3 3D printing specimens tested

the testing procedure for non-instrumented and instrumented method types, is described in two separate parts (Part 1 and Part 2). A hinge break failure mode was observed for 0° and 90° specimens, and brittle fracture for 45° specimens (Figure 3). Deflection–impact force and deflection–impact energy curves were plotted for every specimen and presented in Figures 4 and 5. The results of the specimens printed at 0° are presented in Figures 5 and 6 as S1, S2, and S3. The results of the specimens printed at 90° are S4, S5, and S6. The results of the specimens printed at 45° are presented in Figures 4 and 5 as S7, S8, and S9.

The mean impact strength is 23.98 J/m^2 for specimens at 0° and 31.3 J/m^2 for specimens at 90°, while specimens at 45° are 15.35 J/m^2, as shown in Figure 6.

The average failure impact force for specimens printed at 0° and 90° is 370 N, and 340 N for specimens printed at 45°. The absorbed impact energy of specimens printed at 45° was 0.39 J and for the specimens printed at 0° and 90° the absorbed impact energy was 0.63and 0.81 J, respectively.

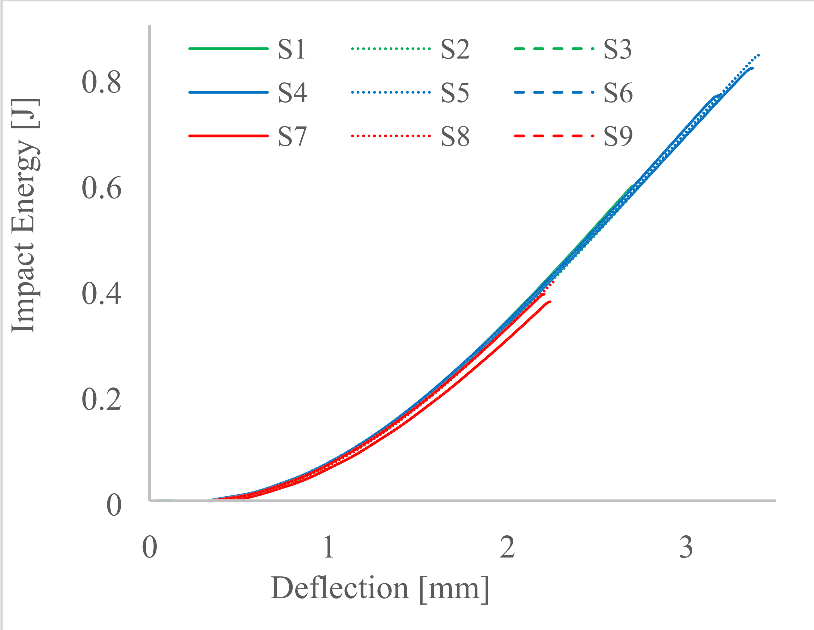

FIGURE 4 Deflection–impact energy curves

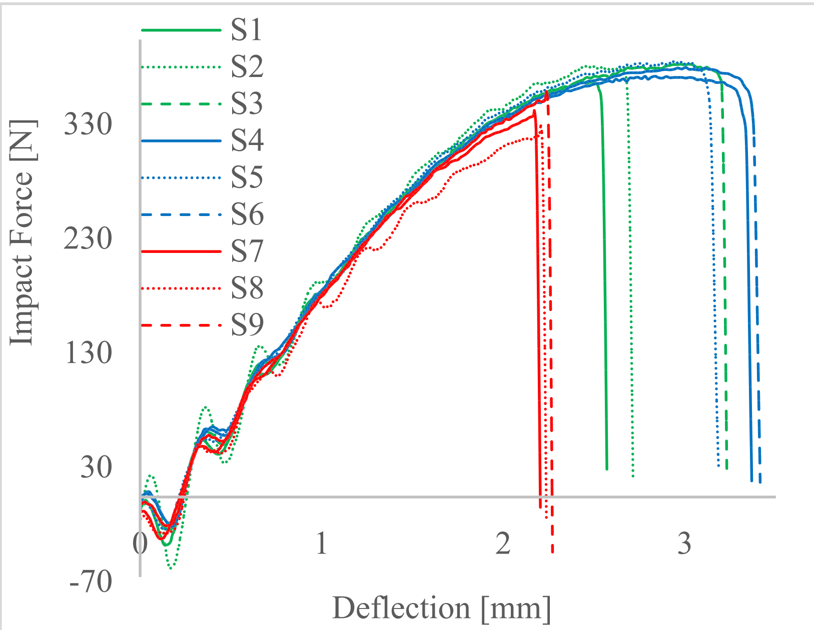

FIGURE 5 Deflection–impact force curves

3 | VIRTUAL TESTING

3.1 | Finite element model of Charpy test

A finite element model was built considering the test specimens' entire geometry, simplified geometry of the impact hammer (striker), contact characteristics, and material fracture conditions, which closely correlated with the physical tests. The numerical simulation of the Charpy test was based on a pendulum impact energy of 5 (J), pendulum weight

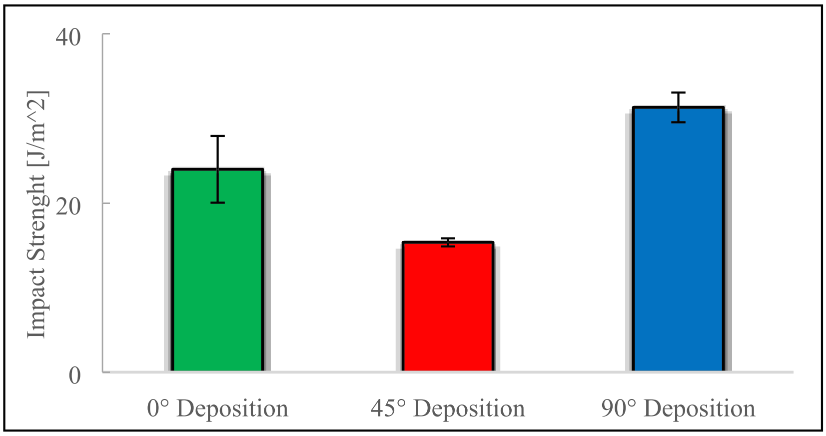

FIGURE 6 Impact strength versus deposition direction

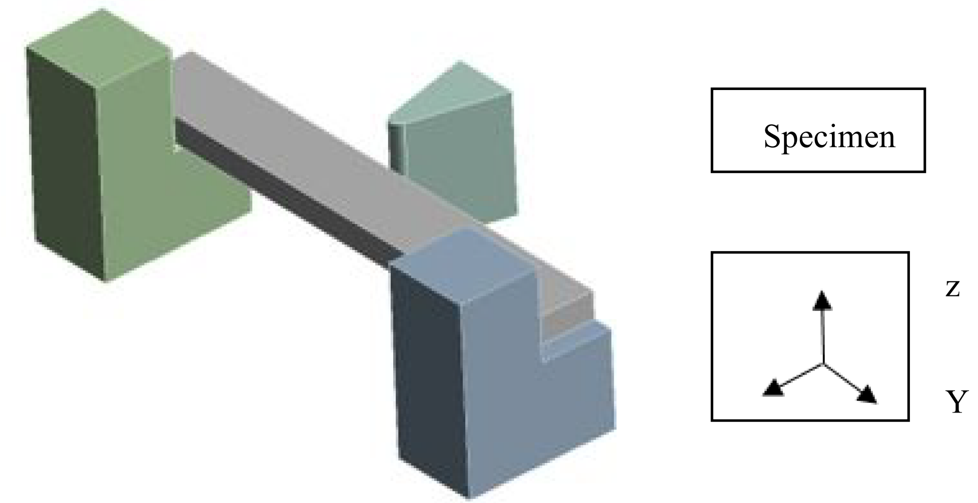

FIGURE 7 Simulation model with boundary conditions

of 1.186 (kg), and an impact velocity of 2.9 (m/s). The material density of the hammer was numerically increased, so the impact kinetic energy of 5 J was achieved.

The numerical model depicted in Figure 7 was discretized using hexahedral first order with reduced integration elements. LS-Dyna Explicit solver, embedded in Ansys Workbench, was used for computation. In this solving technique, nodal accelerations are calculated directly and are entirely determined by their mass and force acting upon them.

Striker and supports were defined as rigid bodies, and all degrees of freedom (DOF) were blocked, except for the Z translation of the striker, to allow applying the initial velocity boundary condition. The geometry was discretized using 59,794 first order, full integrated hexahedral elements of 0.8 mm length, having 15,794 nodes.

3.2 | Material model and failure criteria

The stress–strain curve of the raw ABS material (before printing) was generated using the Ramberg–Osgood equation described in ref.,[16] shown in Table 1 and depicted in Figure 8. An isotropic material model with maximum equivalent strain failure criteria was considered in the simulation model. The strain levels at which failure occurred for each orientation were identified by comparing numerical simulation results against experimental ones. Failure criteria are shown in Table 2.

TABLE 1 Strain at failure for each deposition direction

Young modulus, E	4500 N/mm^2
Ultimate strength	70 N/mm^2
Yield strength	46 N/mm^2
Strain at rupture	20%

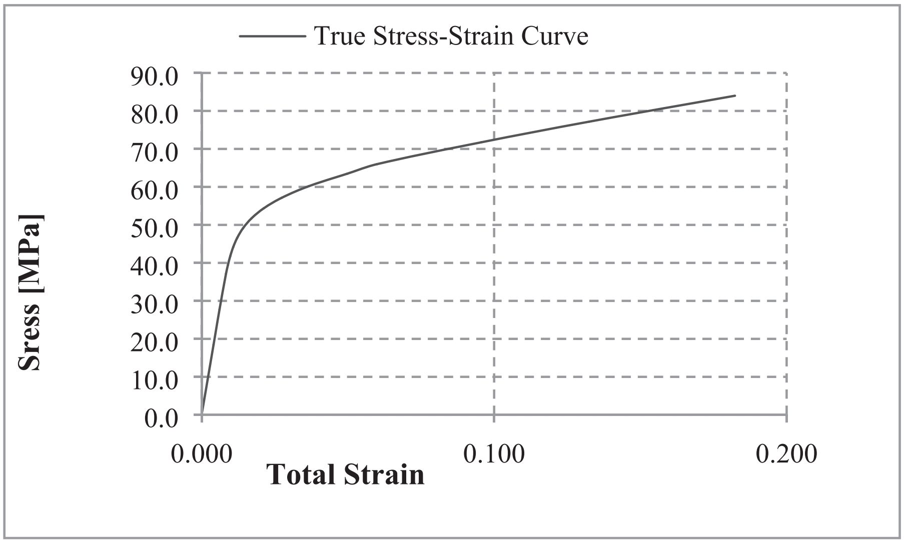

FIGURE 8 ABS true stress–strain curve

TABLE 2 Raw ABS mechanical properties

Deposition direction	Strain at failure (%)
0°	9.5
45°	6
90°	13.2

3.3 | Numerical simulation results compared to physical tests

The correlation between physical tests and numerical simulation are shown in Figure 8. Good agreement was achieved for the energy levels at which breakage occurred, keeping in mind that an isotropic material was used, having only two independent material constants, Young's modulus and Poisson's ratio, which are relatively easy to determine experimentally. The numerical model tends to slightly overpredict the time when the failure occurred. One possible cause for this could be the limitation of the isotropic homogeneous numerical model. The 3D printed part is heterogeneous anisotropic; mechanical properties are location and direction dependent. The outer layers of the test pieces are more brittle than the layer in the middle of the parts, and in the numerical model, all elements are considered isotropic. The difference between experimental and numerical results for the absorbed energy is shown in Figure 9, where the physical tests are considered references. The best correlation was achieved for 45° deposition direction, where there is only a 2% difference between experiments and finite element analysis (FEA) results. For the other two directions, 0° and 90°, the differences are 8% and 5%, which are still in the acceptable range.

The paper presents the results of an experimental investigation carried out on ABS test specimens obtained by AM, having three deposition directions. At the same time, the correlation of the experimental results with the numerical analysis was carried out.

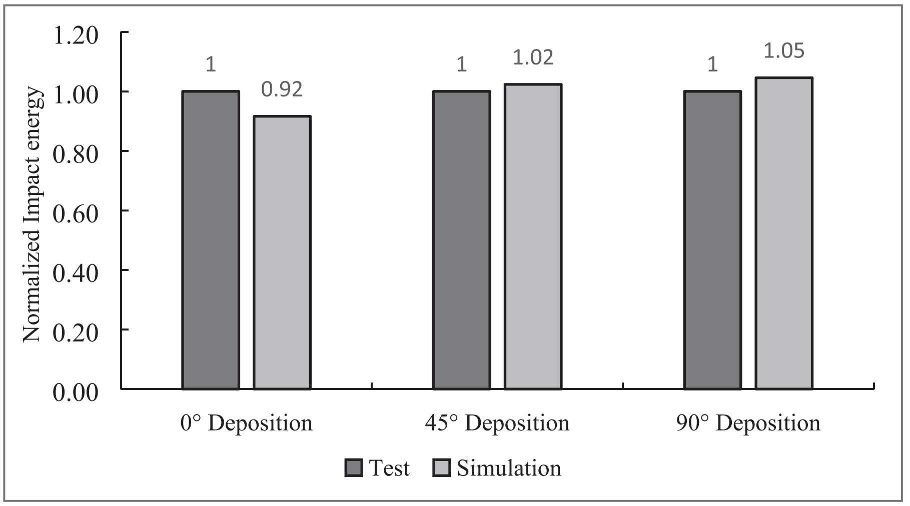

FIGURE 9 Impact energy: numerical versus experimental results

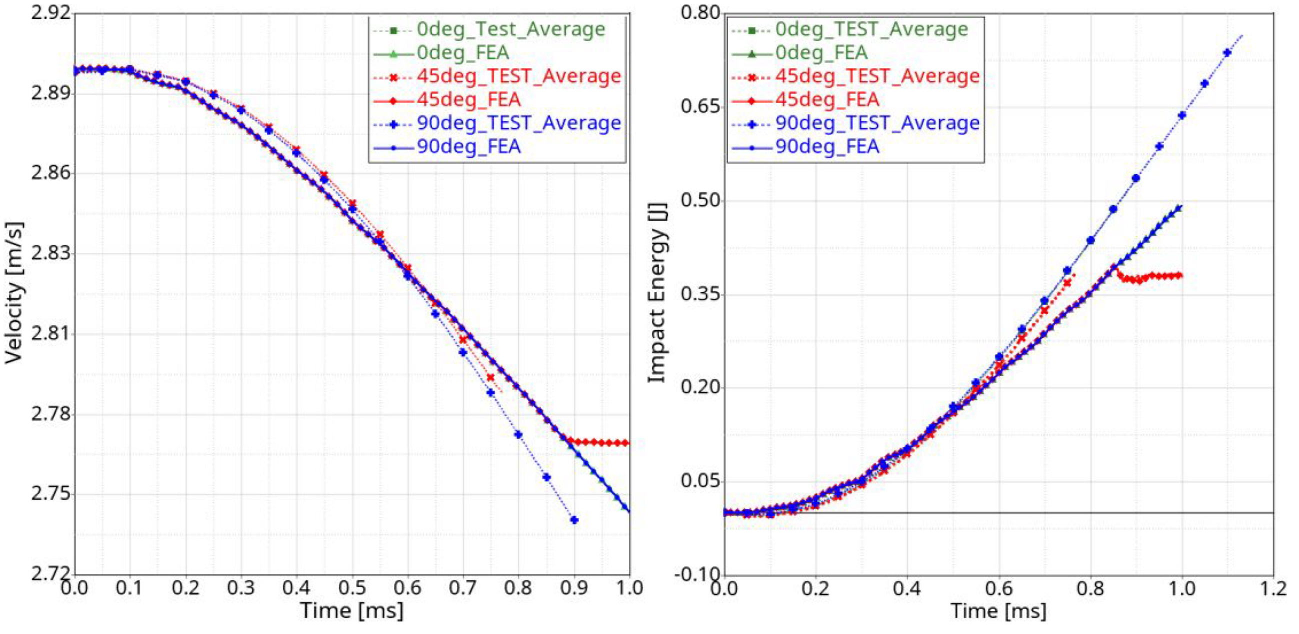

FIGURE 10 Test versus simulation for all deposition directions

The following conclusions could be drawn:

- The average of energy absorbed during impact tests for specimens with the orientation of the layers at 45° was about 0.39 J, and for those with layer orientation at 0° and 90°, was 0.63 and 0.81 J, respectively.
- A hinge break failure mode was observed at 0° and 90° specimens, and brittle fracture for 45° specimens.
- It was observed that the impact strength for 45° printed specimens is half of the impact strength of the specimens printed at 90°.
- Physical testing shown satisfying repeatability for all three deposition directions.
- A good agreement between physical tests and numerical simulations was reached for the absorbed energy levels and velocity (Figure 10) by using three different failure criteria (maximum equivalent strain) levels, one for each deposition direction.

ACKNOWLEDGEMENT

The project leading to this application has received funding from the European Union's Horizon 2020 research and innovation program under grant agreement no. 857124.

DATA AVAILABILITY STATEMENT

The data that support the findings of this study are available from the corresponding author upon reasonable request.

REFERENCES

1. Bilkar D, Keshavamurthy R, Tambrallimath V. Influence of carbon nanofiber reinforcement on mechanical properties of polymer composites developed by FDM. *Mater Today Proc*. 2021;46(10):4559-4562. https://doi.org/10.1016/j.matpr.2020.09.707
2. Parandoush P, Lin D. A review on additive manufacturing of polymer-fiber composites. *Compos Struct*. 2017;182:36-53.
3. Guo P, Zou B, Huang C, Gao H. Study on microstructure, mechanical properties and machinability of efficiently additive manufactured AISI 316L stainless steel by high-power direct laser deposition. *J Mater Process Technol*. 2017;240:12-22. https://doi.org/10.1016/j.jmatprotec.2016.09.005
4. Xing H, Zou B, Wang X, Hu Y, Huang C, Xue K. Fabrication and characterization of SiC whiskers toughened Al2O3 paste for stereolithography 3D printing applications. *J Alloy Compd*. 2020;828:154347. https://doi.org/10.1016/j.jallcom.2020.154347
5. Xing H, Zou B, Liu X. Effect of particle size distribution on the preparation of ZTA ceramic paste applying for stereolithography 3D printing. *Powder Technol*. 2020;359:314-322.
6. Liu X, Zou B, Xing H. The preparation of ZrO2-Al2O3 composite ceramic by SLA-3D printing and sintering processing. *Ceram Int*. 2020;46(1):937-944.
7. Kumar S, Soundararajan R, Shanthosh G, Saravanakumar P, Ratteesh M. Augmenting effect of infill density and annealing on mechanical properties of PETG and CFPETG composites fabricated by FDM composites fabricated by FDM. *Mater Today Proc*. 2020;45:2186-2191.
8. Wang P, Zou B, Ding S, Li L, Huang C. Effects of FDM-3D printing parameters on mechanical properties and microstructure of CF/-PEEK and GF/PEEK. *Chin J Aeronaut*. 2020;34(9):236-246.
9. Fu X, Zhang X, Huang Z. Axial crushing of Nylon and Al/Nylon hybrid tubes by FDM 3D printing. *Compos Struct*. 2021;256:113055. https://doi.org/10.1016/j.compstruct.2020.113055
10. Vălean C, Marşavina L, Mărghitaş M, Linul E, Razavi J, Berto F. Effect of manufacturing parameters on tensile properties of FDM printed specimens. *Proc Struct Integr*. 2020;26:313-320. https://doi.org/10.1016/j.prostr.2020.06.040
11. Razavi S-M-J, Ferro P, Berto F. Fatigue assessment of Ti–6Al–4V circular notched specimens produced by selective laser melting. *Metals*. 2017;7(8):291. https://doi.org/10.3390/met7080291
12. Krausz T, Ailinei I-I, Galatanu SV, Marsavina L. Charpy impact properties and numerical modeling of polycarbonate composites. *Mat Design Process Comm*. 2021;3(4). https://doi.org/10.1002/mdp2.260
13. Benedetti M, du Plessis A, Ritchie RO, Dallago M, Razavi SMJ, Berto F. Architected cellular materials: A review on their mechanical properties towards fatigue-tolerant design and fabrication. *Mater Sci Eng R Rep*. 2021;144:100606. https://doi.org/10.1016/j.mser.2021.100606
14. ISO 179-1, plastics - determination of Charpy impact properties - part 1: non-instrumented impact test, second edition; 2010.
15. ISO 527-2, plastics - determination of tensile properties - part 2: test conditions for moulding and extrusion plastics, second edition; 2012.
16. Ramberg W & Osgood WR Description of stress–strain curves by three parameters. National Advisory Committee For Aeronautics,Technical Note No. 902, Washington DC; 1943.

How to cite this article: Ailinei I-I, Galatanu SV, Marsavina L. The effects of layers orientation on impact energy evaluation of FDM printed specimens. *Mat Design Process Comm*. 2021;3(6):e267. doi:10.1002/mdp2.267